Research Square

Preprints are preliminary reports that have not undergone peer review.
They should not be considered conclusive, used to inform clinical practice,
or referenced by the media as validated information.

Comparative spatial transcriptomic profiling of canine and human lung metastatic osteosarcoma tumor microenvironments

Daniel Regan

Daniel.Regan@colostate.edu

Rebecca Makii
Kathryn Cronise
Colorado State University
Michael McKenna
Maria Hernandez
Noemi Kedei
Jennifer Cotter
Troy McEachron
National Cancer Institute

Article

Keywords: canine, osteosarcoma; tumor microenvironment, macrophages, tumor immunity

Posted Date: November 6th, 2026

DOI: https://doi.org/10.21203/rs.3.rs-11224412/v1

License: This work is licensed under a Creative Commons Attribution 4.0 International License.
Read Full License

Additional Declarations: There is **NO** Competing Interest.

Comparative spatial transcriptomic profiling of canine and human lung metastatic osteosarcoma tumor microenvironments

Running title: Comparative spatial transcriptomic profiling of canine and human lung metastatic osteosarcoma tumor microenvironments

Keywords: *canine, osteosarcoma; tumor microenvironment, macrophages, tumor immunity*

ABSTRACT

Osteosarcoma (OS) is a rare pediatric cancer with poor outcomes due to metastases. These outcomes are mirrored in the spontaneous canine disease, offering a comparative opportunity to understand disease progression and tumor immunology. Studies have identified overlaps in molecular features between species, bolstering the utility of the canine model. With the introduction of cross-species-compatible spatial transcriptomics, there is unprecedented opportunity to dissect the metastatic OS tumor microenvironment through comparative oncology.

This study identified conserved cellular signals in metastatic OS through independent and integrated analyses of canine (n=7) and human (n=5) GeoMx spatial transcriptomic datasets. Macrophage (CD163+ or CD68+), T cell (CD3+), and negative (CD163-/CD3- or CD68-/CD3-) tumor/stroma compartments were captured from intratumoral and peritumoral regions. Data were analyzed independently using GeomxWorkflows and integratively with Seurat, focusing on orthologous genes.

We identified spatially dependent differences in tumor-associated T cell and macrophage infiltrates and conserved regional immune heterogeneity across canine and human metastatic OS, further strengthening the translational capabilities of the canine model. Shared features include upregulation of a JAG1-Notch signaling within macrophages, metabolic alterations in T

cells, and increased MIF expression. These conserved pathways provide a foundation for investigating mechanisms contributing to metastatic OS progression and intratumoral immunosuppression.

INTRODUCTION

Osteosarcoma (OS) is the most common primary malignant bone tumor in humans and dogs [1,2]. Despite aggressive treatment, up to 40% of human and over 90% of canine patients succumb to multi-drug-resistant metastatic disease, most commonly impacting the lungs [3–5]. OS is a rare pediatric cancer but has a greater than 10-fold increased incidence in canine companion animals, permitting enhanced access to patient-derived samples, novel opportunities for preclinical modeling, and accelerated drug development in a naturally occurring, and immune intact disease context [2,6]. Prior foundational research has shown that canine OS demonstrates remarkable similarities in clinical presentation, histopathological appearance, and molecular aberrations to its human counterpart, positioning the dog as a translationally relevant model to accelerate our understanding of conserved molecular features and potential therapeutic target discovery for OS [1–3,7–9]. By leveraging both human and veterinary OS patient cohorts and specimens, there is greater opportunity to comparatively investigate conserved disease mechanisms, identify candidate therapeutic targets and/or biomarkers, and evaluate therapeutic strategies which have relevance across both species.

The past few decades of OS research have been primarily focused on tumor cell-intrinsic mechanisms of metastasis and drug resistance. However, despite discovery of intrinsic molecular drivers of OS and promising studies demonstrating efficacy of immune checkpoint and molecular targeted therapies in rodent models, this has not translated into clinical effectiveness [2,7,10]. These observations highlight a disconnect between preclinical and clinical efficacy, likely due in part to our lack of understanding of the complexity of the OS tumor microenvironment (TME) and potential failure of current rodent models to recapitulate this complexity. Together, this has shifted recent investigations towards understanding how non-malignant cells of the TME promote OS progression.

Significant advancements in spatially resolved multi-omic technologies have enabled molecular profiling of the TME at unprecedented resolution [11–13]. However, few established frameworks exist for spatial analyses in comparative oncology, in part, due to limited non-human probe-based platforms and the requirement of fresh frozen specimens for species agnostic methods, which can be technically challenging to perform on unfixed harder mineralized tissues such as OS. However, the introduction of the probe-based Canine Cancer Atlas for utilization with Bruker's (formerly Nanostring) GeoMx Digital Spatial Profiler (DSP) has enabled spatially resolved cell-type specific gene expression profiling of formalin-fixed paraffin embedded (FFPE) tissue specimens. This technology was recently successfully employed to profile primary appendicular canine OS tumor tissue, identifying conserved targetable pathways also described in human OS [14].

In this study, we leverage the GeoMX DSP technology for evaluation of spatially dependent changes in tumor-associated T cell and macrophage infiltrates in canine lung metastatic OS samples, further validating the utility of this platform for spatial transcriptomic profiling of canine cancers. Moreover, we demonstrate a method of cross-species GeoMx spatial transcriptomic data integration which highlights conserved cell-type and location-specific gene expression patterns, phenotypes, and pathways of immune suppression in canine and human OS lung metastases.

MATERIALS & METHODS

Canine metastatic osteosarcoma tissue samples

Formalin-fixed paraffin embedded (FFPE) tissue specimens from canine patients with a histologically confirmed diagnosis of metastatic pulmonary osteosarcoma between 2015-2022 were obtained from the Veterinary Diagnostic Laboratory tissue archive at Colorado State University (CSU). All samples were obtained from routine diagnostic necropsy (generally

performed within < 24 hours of death) or biopsy and archived with informed owner consent in compliance with the Institutional Animal Care and Use Committee at CSU. Detailed patient demographics are available in supplemental data S1. Confirmation of tumor and surrounding non-malignant tissues were assessed with a single hematoxylin and eosin (H&E) stained slide by two board certified veterinary pathologists. Specimens were excluded from the study if there was poor cellularity, substantial necrosis, hemorrhage, tissue fragmentation and/or folding. A total of 41 canine specimens were identified for additional processing.

RNA Isolation and canine IO gene expression profiling

Canine samples were first assessed for their RNA-binding probe hybridization capacity by nCounter using the Canine IO Panel (800 canine specific genes). Nucleic acids were isolated using the AllPrep DNA/RNA FFPE Nucleic Acid Extraction kit (Qiagen) from either two 10 um FFPE curls or ~3-5 unstained FFPE slides with macrodissection to ensure at least 80% of the sample input was composed of tumor. RNA sample quality and concentration were measured by RNA ScreenTape (Agilent) or Qubit RNA Broad Range assay (Invitrogen), respectfully. RNA from all 41 samples was run on an nCounter Sprint Profiler with panel standards for batch correction. Acquired RCC files were processed with the nSolver software (v4.0) via previously published protocols for quality control assessment, background thresholding, and normalization [15]. All samples demonstrated successful probe hybridization. Seven canine specimens of excellent histologic quality were pursued for spatial transcriptomics.

Human case acquisition and quality assessment

Archived FFPE specimens from pediatric patients with metastatic pulmonary osteosarcoma were obtained from the Department of Pathology at Children's Hospital Los Angeles under Institutional Review Board protocol CCI12-00224. Specimen clinical attributes

can be found in supplemental data S1. Serial 5 μm sections from each block were collected. One slide was stained with H&E to confirm tumor presence and assess sample integrity as described above for canine specimens. To confirm samples could successfully hybridize with RNA-binding probes, RNAscope was performed using the RNAscope 2.5 Assay (ACD Bio) using probes against *GAPDH* (ACD Bio, #310321-C2) according to the manufacturer's protocol. A total of five samples were used for spatial profiling.

GeoMx Digital Spatial Profiling (DSP)

Canine FFPE samples (n = 7 metastases) were sectioned at 5 μm and macrodissected on a water bath based on tumor-containing regions identified by two board-certified veterinary anatomic pathologists (RLM, DPR) prior to placement on positively-charged slides. Up to 4 samples were placed on two slides for analysis. Canine samples were analyzed with GeoMx DSP using the Canine Cancer Atlas panel (1,962 canine-specific genes) in collaboration with the Technology Access Program at Nanostring, Seattle, WA. Human FFPE samples (n = 5 metastases) were sectioned at 5 μm thickness onto APEX-treated slides to enhance tissue adherence. Each slide, representative of one patient sample, was analyzed with GeoMx DSP using the Human Whole Transcriptome Atlas (18,815 human-specific genes) in collaboration with the Spatial Technologies Resource at the Research Technologies Branch (Bethesda, MD).

For the canine samples, morphology markers for segmentation included CD163, CD3, and SYTO 83. With pathologist supervision, each sample had at least one intratumoral tumor core region of interest (ROI) and one peritumoral tumor margin ROI collected. Three samples had an additional peritumoral, non-tumor containing lung ROI acquired. For all ROIs, three areas of illumination (AOI) were acquired: CD3+ T cells, CD163+ macrophages, and CD3-CD163- remaining "Negative" stromal tissue. For human samples, morphology markers for segmentation included CD68, CD3, and SYTO 13. Representative ROIs were selected from intratumoral and peritumoral regions in the human samples based on tissue morphology to

collect regions with morphology-based masking. A total of 51 AOIs were obtained from 18 ROIs for the canine samples and 137 AOIs were obtained from 69 ROIs in the human samples.

For GeoMx DSP, briefly, FFPE slides were baked overnight at 60°C, followed by deparaffinization and antigen retrieval on a Leica BOND RX automated stainer. Antigen retrieval was performed using HIER2 (EDTA-based antigen retrieval solution) for 20 min, followed by proteinase K treatment (1 µg/mL) for 15 min at 37°C, according to NanoString recommendations. Species appropriate probes were applied to the tissue sections and hybridized for 20 h at 37°C. Following hybridization, slides were washed twice with stringent wash solution (50% formamide in 2× SSC) for 25 min per wash, followed by two washes with 2× SSC for 2 min each. Slides were blocked with W buffer for 30 min and incubated with appropriate morphology antibodies (see supplemental S2) all prepared in W buffer. Slides were then washed three times with 1× SSC for 5 min each. Slides were scanned using the GeoMx DSP for visualization and selection of ROIs. Within selected ROIs, oligonucleotide barcodes were released by UV photocleavage, collected into 96-well plates, and processed for library preparation and sequencing according to the NanoString GeoMx NGS protocol or prepared for nCounter processing .

For NGS samples (human), libraries were pooled and quantified on the Illumina iSeq100 to confirm sample presence and pooling ratios. Final sequencing was performed on an Illumina NovaSeq 6000 using a S4/XP-2 lane flow cell with 27 × 27-bp reads and 8 × 8-bp index reads. Raw base-call files were demultiplexed into ROI-specific FASTQ files using BCL Convert software. FASTQ files were subsequently processed using the NanoString GeoMx NGS Pipeline (v2.3.3.10) to generate Digital Count Conversion (DCC) files for downstream analysis.

Acquired DCC files were processed and analyzed with GeomxTools (v3.10.0) in R. Canine and human datasets were processed, filtered, and Q3 normalized in parallel with default quality control parameters as recommended by the manufacturer (Supplemental Figures 1-4). ROI which failed quality check due to technical dropout were excluded. In select samples, few

QC warnings were attributed to low immune cell infiltrate rather than technical dropout due to relevant immune cell transcripts demonstrated to be expressed above background, thus these AOIs were maintained in downstream analyses.

Deconvolution of cell subsets using custom scRNAseq annotations

To estimate the relative proportion of different cell types, the SpatialDecon package (v1.16.0) in R was utilized [16]. Custom matrices were generated using annotations derived from a publicly available integrated scRNAseq canine and human metastatic OS atlas [17]. Macrophage and T cell spatial datasets utilized subclustered macrophage and T cell specific scRNAseq annotations, whereas “Negative” regions used broad major cell identity clustering annotations (supplemental data S3-5). Bar plots of cell type abundance were plotted with TIL_Barplot. Relative proportions were compared between intratumoral and peritumoral regions and significance was evaluated by Welch’s t-test with Holm-Sidak correction (GraphPad Prism v11).

Independent GeoMx data analysis and statistical analysis

To compare GeoMx experiments across species, Q3 normalized human data were indexed to only include orthologous genes between the canine and human panels prior to differential gene expression analysis. Canine gene loci which were undefined at the time of panel development were cross-referenced with NCBI RefSeq and manually updated into a locus dictionary (supplemental data S6). Panel overlap is represented in Figure 1b and full gene lists for each panel are available in supplemental data S7-8.

In both datasets, differentially expressed genes (DEGs) from intratumoral and peritumoral ROIs were evaluated based on Q3 normalized expression values from each AOI. DEGs were evaluated using a linear mixed-effects model with a random slope using the

mixedModelDE function in the GeomxTools package (v3.10.0) with Benjamin-Hochberg (BH) correction for multiple comparisons as recommended by the manufacturer. Significant DEGs were defined as p value < 0.05 and fold change of ± 1.5 (equivalent to log2 fold change ± 0.58).

Canine and human GeoMx data integration and statistical analysis

To create a combined dataset, both canine and human datasets were first indexed to only include overlapping genes after independent normalization. GeoMx datasets were then converted into Seurat objects with GeomxTools (v3.10.0). Seurat objects were first evaluated as a merged dataset with JoinLayers. Results were then integrated using the IntegrateLayers function and anchor-based RPCA and CCA integration strategies with k.weight = 29. Unsupervised clusters from each integration method were evaluated by dimensionality reduction.

To compare integrated DEG evaluation to independent DEG analyses, intratumoral and peritumoral ROIs were evaluated using the FindMarkers function in Seurat (v5.3.0) using default parameters (non-parametric Wilcoxon rank sum with BH correction for multiple comparisons). Significant DEGs were defined as p value < 0.05 and fold change of ± 1.5. GSEA on the integrated dataset was performed with fgsea (v1.32.4) using all Gene Ontology (GO), Reactome, and WikiPathways gene sets.

To compare shared gene trends between species, DEG datasets were merged based on gene identifiers and restricted to matching AOI cell phenotype segments (e.g. canine CD3+ T cell segments and corresponding human CD3+ T cell segments). Results were filtered to demonstrate genes with significant p-values and overlapping DEGs were visualized with UpSetR (v1.4.0) in R. Gene set enrichment analysis (GSEA) was performed on each dataset using genes ranked by model coefficient estimate and filtered to only retain those with a nominal p-value < 0.05. The resulting pre-ranked gene lists were used as input for fgsea (v1.32.4) using GO, Reactome, and WikiPathways gene sets and subcollections.

RESULTS

Experimental and analytical overview is represented in Figure 1a.

Species integration of GeoMx data with Seurat preserves distinct cell phenotypes and enhances T cell characterization

In order to understand both conserved and species-specific differences in how microanatomical location within the metastatic OS TME influences T cell and macrophage phenotype, we first sought to integrate our canine and human GeoMx datasets for combined differential gene and pathway enrichment analysis. To do this, we utilized Seurat V5 due its previously reported ability to handle spatial data and ease of GeoMx to SeuratObject conversion [18]. After datasets were indexed on overlapping orthologs and converted into Seurat objects, initial merging of datasets via Seurat demonstrated strong clustering driven by species (Figure 2a). We hypothesized this clustering was, in part, associated with batch effect. Therefore, integrative analysis was performed on the datasets using two inbuilt anchor-based methods (CCA and RPCA), which are widely used for transcriptomic dataset integration, including in cross-species applications [19,20]. Seurat V5 RPCA integration demonstrated excellent interspecies integration of spatial datasets while maintaining meaningful biologic preservation of major cell identities (Figure 2b).

Unsupervised RPCA clustering of the integrated data identified 8 distinct clusters (Figure 2c). Relative cell proportions for each RPCA cluster are demonstrated in Figures 2d and 2e based on Cell Type and tumor ROI proportions, respectively. Cluster 0 was mostly comprised of CD163+ or CD68+ macrophage AOIs. Clusters 1, 4 & 6 were predominantly CD3+ AOIs from both species. Clusters 2, 3, 5 and 7 all represented predominantly “Negative” regions. Cluster 3 represented predominantly peritumoral “Negative” regions, most consistent with surrounding pulmonary parenchyma whereas clusters 2, 5 & 7 were predominantly intratumoral, suggesting

greater composition of tumor cells and associated stroma. Of note, cluster 5 was almost entirely derived from a single case and formed a cluster most separate from the others. Interestingly, this sample was the only fibroblastic OS histological subtype included in our dataset, suggesting this subtype has distinct transcriptional differences from osteoblastic or chondroblastic subtypes. In line with this observation, this case was previously published in a Visium dataset and also demonstrated divergent transcriptional profiles [21].

Unsupervised clustering demonstrated three distinct clusters of T cells (clusters 1, 4 & 6). Cluster 1 was characterized by expression of markers associated with cytotoxic effector cells including *CD8A, NKG7, GZMK, FALG* and *KLRK1* (NKG2D). This cluster had the highest proportion of intratumoral T cells compared to other T cell clusters. The predominance of intratumoral T cells in this cluster was histologically confirmed to be driven by the singular fibroblastic subtype sample. To account for this, region proportions were calculated solely with the remaining T cells in this cluster and were subsequently identified to be primarily enriched in the peritumoral compartment (Supplemental Figure 5). These findings align with region proportions from the other T cell predominating clusters 4 and 6 and other studies which have demonstrated that OS metastases often exhibit intratumoral T cell exclusion [22,23].

Cluster 6 lymphocytes demonstrated relatively increased expression of costimulatory or regulatory checkpoint molecule expression consistent with T cell activation including *CTLA4*, *ICOS* (CD278), *CD276* (B7-H3), *CD5* and *CD6*. These cells were also preferentially enriched in the peritumoral location. Cluster 4 was also associated with our CD3+ AOIs and was defined by expression of canonical T helper cell associated genes such as *IL17RB*, *TRAT1*, and *IL2*. Interestingly, this cluster also expressed myeloid associated genes including *TNFSF13B* (BAFF) and *IL27*, potentially reflective of cellular overlap not appreciated on morphology marker imaging and region selection or close cell-cell contact such as immune synapse formation between T cells and neighboring professional antigen-presenting cells, given the MHC II

restriction of CD4 helper T cells. This lymphocyte cluster also had the highest proportion of peritumoral representation.

While both peritumoral and intratumoral macrophages were represented in cluster 0, peritumoral macrophages were predominant. This cluster was characterized by common macrophage surface receptor expression like *CD163*, *MSR1*, *MRC1* (CD206), and *FCER1G*. Cells from this cluster also expressed *CTSS* (cathepsin S), noted to be involved in ECM remodeling and fibrosis [24]. Interestingly, this cluster demonstrated residual species effect, with slight sub clustering of canine and human samples. This may be related to the limitations of available pan-macrophage antibodies for dogs, reflecting differences in AOI collection obtained from CD163+ cells versus CD68+ cells. Additionally, a subset of macrophage AOIs clustered within either T cell or “Negative” dominant clusters (Figure 2b) which may indicate areas with increased macrophage cell-cell interactions and thus, diminished cell segmentation, highlighting some technical limitations of the GeoMx assay.

Clusters 2 and 7 predominantly represented “Negative” intratumoral ROIs and were characterized by abundant ECM-associated genes. Interestingly, fibroblast-associated markers such as *FGFR1*, *NOTCH3*, and *WNT5A* were predominant in cluster 2 whereas cluster 7 had a broader array of cancer associated genes including *MYC*, *CD276* (B7-H3), and *PDGFA*. Cluster 3 predominantly represented “Negative” peritumoral ROIs, and the transcriptional signatures support mixed pulmonary parenchyma including epithelial markers like *AXIN2*, *EPCAM*, and *LAMA3*, Type II pneumocyte marker *LAMP3*, and canonical endothelial marker *CDH5*.

Overall, integration of canine and human spatial datasets demonstrates strong cell-type specific unsupervised clustering and may be considered a useful mechanism to explore conserved cellular pathways across species.

Cell deconvolution demonstrates regionally distinct and highly heterogenous cell populations shared between canine and human metastatic OS

Deconvolution utilizing macrophage annotations derived from a multi-species metastatic OS RNASeq atlas exhibits intratumoral enrichment for fibrogenic and osteoclast-like TAMs (Figure 3a). Interestingly, these osteoclast-like TAMs were previously identified to exist in discrete intratumoral pockets, and we similarly identify their intratumoral localization [17]. Their relative proportion was most prominent in human samples, which may be associated with species-specific differences in our macrophage marker selection. Peritumoral macrophages had higher proportions of alveolar macrophages, which is most prominently highlighted in the human dataset, likely due to CD68 serving as a broader pan-macrophage marker compared to CD163 in our canine samples. Similar analyses conducted with T cell populations demonstrate intratumoral enrichment for proliferating T cells and peritumoral enrichment for CD8+ effector T cells (Figure 3b). These data suggest there are distinct regional differences associated with T cell transcriptional profiles within OS metastases. Although an infrequently observed population, Tregs were largely confined to the peritumoral environment when detected. Remaining relevant annotations within the multi-species metastatic OS RNASeq atlas were applied to the “Negative” dataset. In our canine “Negative” dataset, there is intratumoral enrichment for Metabolically Primed (MP) Progenitor tumor cells, which constitute most of the intratumoral cell population and are characterized by their metabolic reprogramming and stem-like state. In our human dataset, “MP Progenitor” tumor cells are also the most abundant tumor population; however, our data demonstrate that when looking at all cell populations within the intratumoral “Negative” regions, cancer associated fibroblasts (CAFs) are the most abundant cell population overall (Figure 3c). This finding may be related to the inclusion of a fibroblastic histotype in human dataset, but a spatially distinct difference in TME composition between species cannot be entirely excluded. For both canine and human samples, CAFs contributed to the greatest proportion of peritumoral “Negative” cells. This is an interesting finding when coupled with the

intratumoral enrichment for fibrogenic TAMs, suggesting an intratumoral environment characterized by robust extracellular matrix programs.

Intratumoral macrophages are enriched for pro-tumorigenic JAG1 in both canine and human metastatic OS

Integrated analyses demonstrate that intratumoral macrophages are enriched for pathways related to ossification and extracellular matrix (ECM) organization driven by high expression of *SPP1* (osteopontin), *YAP1*, *SPARC*, and *BMP4* (Figures 4a-c). Interestingly, the genes driving these pathways are also overwhelmingly associated with pro-fibrotic and/or immunosuppressive macrophage subtypes observed in other lung metastatic TMEs and idiopathic pulmonary fibrosis [25–30]. Notably, both *SPARC* and *BMP4* are demonstrated to be upregulated or implicated in osteosarcoma progression [31,32].

Comparing integrated analyses with independent DEG analyses of human (Figures 4d-e) and canine (Figures 4f-g) samples, four conserved significant DEGs in intratumoral macrophages are identified across all analyses: *JAG1*, *CDH11*, *FGFR1*, and *MMP14* (Figure 4h and 4i). Collectively, these four genes corroborate the integrated pathway enrichment analysis for intratumoral macrophages and converge around a central theme of a stromal interacting and pro-angiogenic TAM population involved in active tissue/ECM remodeling. Interestingly, JAG1, a canonical Notch pathway ligand with known oncogenic properties in many different cancers, including osteosarcoma, was also recently associated with macrophage mediated chemoresistance [33–35]. Though only appearing in the integrated dataset, *CSF1R* also arises as a DEG in intratumoral macrophages. CSF1R targeted therapy to reprogram intratumoral macrophages is currently being explored in sarcomas, and this finding suggests this may be a conserved target in both canine and human metastatic OS [36].

Peritumoral macrophages in our dataset exhibit robust inflammatory pathway enrichments, including “defense response” and “immune response” characterized by upregulation of *MARCO, IRF5*, *MYD88*, and *LYZ*. This phenotype is most consistent with a tissue resident but tumor-activated alveolar macrophage. The “defense response” pathway has been specifically described in human metastatic pulmonary OS lesions supporting an immunologic response similar to that of a foreign body injury [21]. Our data further supports this finding by demonstrating conserved pathway enrichment across both canine and human pulmonary metastases.

Conserved expression of immunosuppressive N5TE (CD73) and LGALS1 (Gal-1) in intratumoral T cells

Immune-matrix interactions are enriched in our integrated intratumoral T cell dataset, including enrichment for “extracellular matrix binding”, “wound healing spreading of cells”, and “collagen-containing extracellular matrix” pathways (Figures 5a-c). Key genes driving these pathways include *CD44*, the primary hyaluronic acid receptor, and *LGALS1* (Gal-1), an autoimmune regulatory protein. Both genes were most striking in the human-derived samples, notably driven by a single fibroblastic subtype patient (Figure 5i). Additional sampling would be required to determine if these findings reflect true species or histological subtype-specific differences. When this subtype is removed from analysis, CD44 becomes a peritumoral DEG while LGALS1 remains as an intratumoral DEG (Supplemental Figure 5).

The canonical glycolysis pathways were also specifically upregulated in intratumoral T cells and intratumoral tumor/stroma (Figure 5b). Metabolic reprogramming towards primary glucose utilization is well-characterized for both T cell activation and tumor cell survival [37,38]. Though there is limited overlap of our integrated and independent DEG analyses in human (Figures 5d-e) and canine (Figures 5f-g) samples, the immunosuppressive checkpoint N5TE

(CD73) appears as an intratumoral T cell DEG in all datasets (Figure 5i). The immunosuppressive properties of CD73 are associated with its regulation of adenosine metabolism, effects which can be amplified by the generally hypoxic and glycolytically skewed TME [39,40]. This marker is most frequently expressed on regulatory, memory, and effector T cell populations [41–43]. However, deconvolution analysis (Figure 3b) demonstrated that proliferating and/or CD8 T cells are the principal intratumoral T cell population in both canine and human metastases, suggesting this marker is most likely associated with an effector memory population of intratumoral CD8 T cells in our dataset. Interestingly, the profibrotic and immunoregulatory cytokine TGFβ, which is significantly enriched in lung metastases, has been previously reported to induce expression of CD73 on CD8+ anti-tumor T cells as a mechanism of resistance to agonistic co-stimulatory receptor [21,44,45]. Of note, in our integrated dataset, the fold change (1.48) for N5TE expression is just below our threshold cutoff but meets this cutoff in independent analyses of both species, demonstrating value in considering both integrated and independent spatial dataset analyses in cross-species studies.

Peritumoral T cells were enriched for pathways associated with leukocyte migration and chemotaxis, driven by genes like *CCR6* and *CCR4,* and likely consistent with recent extravasation into the metastatic OS TME [46,47]. These results correlate with peritumoral enrichment for the chemokine CCL20, the ligand for CCR6, in both macrophage and “Negative” compartments in our dataset. CCR6 has been demonstrated to be integral for Th17 and Treg recruitment, suggesting this axis may serve as an additional mechanism for immune evasion in the metastatic pulmonary OS TME [46,47]. Similarly. CCR4+ T cells are often associated with Th2, Th17 or Treg subsets [48]. Interaction with its ligands CCL17 and CCL22 can also contribute to Treg-mediated immune evasion in cancers [49]. Interestingly, both CCL17 and CCL22 were significantly enriched peritumorally in the “Negative” and CD3 compartments, respectively.

The intratumoral OS TME is uniquely enriched for the pro-inflammatory and pro-tumorigenic cytokine MIF

Intratumoral “negative” regions, representing metastatic OS tumor cells, stroma, vasculature, and CD3-/CD68- or CD3-/CD163- immune cells, are enriched for “endochondral ossification”, “osteopontin signaling”, “transcriptional regulation by RUNX2”, and “collagen metabolic process pathway” among other ECM-related gene sets (Figures 6a-c). While these pathways are consistent with key diagnostic features of OS, namely osteoid and ECM production, they are also reflective of recently described hallmarks of OS tumor cell and metastasis biology. RUNX2 has been recently reported to define a transcriptionally distinct molecular subtype of human OS while SPP1 (osteopontin) signaling has been shown to be a driver of metastasis across several different cancers [50–53]

Intratumoral “negative” regions demonstrated the most DEG overlap compared to T cell/macrophage-enriched regions between integrated and independent analyses in human (Figures 6d-e) and canine (Figures 6f-g) samples, with overlaps highlighted in Figure 6h. Of the six total genes (AURKB, CDC20, GPI, MAD2L2, MCM5, MIF) demonstrated to be upregulated intratumorally, macrophage migration inhibitory factor (MIF) stands out as another potential immunological target for metastatic OS. This observed upregulation of MIF in our dataset is consistent with a recent report demonstrating MIF upregulation at both the RNA and protein level in the intratumoral compartment of human lung metastatic OS tissues and OS patient-derived cell lines [21]. In addition to its tumor intrinsic effects of sustaining tumor cell survival and proliferation through autocrine MIF driven activation of NFkB, MYC, PI3K/Akt, and ERK signaling pathways, cancer cell secreted MIF has also been reported to shape the TME of various solid tumors through mediating immune suppressive TAM polarization and myeloid-derived suppressor cell recruitment [54–56]. These data suggest that MIF may represent an

opportunity for dual tumor and TME compartment targeting in OS, and that canine OS may be a valuable naturally occurring model for testing such a therapeutic approach.

In contrast, the peritumoral “negative” environment is enriched for immune-related chemotactic signals and immune response pathways driven by genes like *IL7R*, *LYZ* (lysozyme), and *SELL* (L-selectin). Though the IL7R is best characterized for T cell development, it has also been described to play a role in B cell function and myeloid homeostasis and can also be expressed on activated fibroblasts in inflammatory conditions, potentially accounting for its upregulation within this “negative” AOI compartment and not the CD3+ cell compartment [57–59]. Similarly, lysozyme is a key marker of resident alveolar macrophages (AMs), and its upregulation in this “negative” compartment is likely reflective of expression in a subset of $CD163^{Neg}$\$CD206^{Neg}$ AMs [60,61]. L-selectin is an integral cell adhesion molecule broadly expressed across all leukocytes during migration into inflamed tissues, likely accounting for its upregulation in this ‘negative’ AOI compartment, and further corroborating enrichment of inflammatory signaling localized to the peri-tumoral region of OS lung metastases [62,63].

Collectively, these findings suggest that the intratumoral environment of lung metastatic OS is one of immune suppression driven by gene and pathway signatures suggestive of pro-fibrosis/ECM remodeling, myeloid cell chemoattraction, TAM and Treg enrichment and effector T cell suppression. In contrast, the peritumoral pulmonary microenvironment demonstrates robust upregulation of genes and pathways associated with chronic inflammatory signaling reflective of an attempted anti-tumor immune response to OS and consistent with previously reported multiplex IHC spatial analyses of metastatic OS [21,22]

DISCUSSION

Though considered a relatively rare cancer in humans, osteosarcoma occurs with at least a 10 times greater frequency in companion dogs [1,2]. The conserved molecular, clinical, and histopathologic features between canine and human OS have positioned the dog as a translationally relevant model to understand OS pathogenesis and treatment susceptibilities [9]. In both species, clinical challenges can exist for obtaining adequate fresh tumor tissue from metastatic sites such as the lung sufficient in amount for deep molecular profiling with advanced multi-omic techniques. While metastasectomies are part of standard-of care for human OS, these surgeries are not routinely performed in veterinary oncology patient care. Thus, technologies which can utilize archived FFPE tissues allow for greater access and multi-use flexibility for patient sample profiling, particularly for rare diseases like osteosarcoma. As such, we performed GeoMX spatial transcriptomic analysis on canine and human FFPE OS lung metastases in order to demonstrate the validity of this platform for cross-species dataset integration, analysis and investigation of mechanisms of OS metastatic progression. Notably, there are few studies which have evaluated cross-species integration of spatial datasets, and most have focused on its utility in brain atlas development and/or cross-platform integration rather than within comparative oncology [64,65]

Using this approach, we demonstrate there is regionally distinct immune cell heterogeneity that is conserved between canine and human OS lung metastases. We also specifically identify upregulation of a JAG1-Notch signaling pathway within intratumoral macrophages, metabolic alteration of intratumoral T cells, and intratumoral upregulation of the pleiotropic pro-metastatic cytokine MIF. Importantly, these pathways may demonstrate cross-species conserved, coordinated mechanisms of metastatic progression and immunosuppression in OS and may represent targetable pathways for reversing these tumor promoting properties of the metastatic OS TME.

JAG1-NOTCH signaling within the TME has been demonstrated to exhibit pro-tumorigenic properties including inhibiting apoptosis, enhancing angiogenesis, and promoting differentiation of CD4+ T cells towards more pro-tumorigenic subsets including Th2, Th17, and especially Tregs [33,66]. While macrophage-derived JAG1 expression has not been previously reported in OS, the robust intratumoral macrophage expression of JAG1 with concurrent NOTCH2 and NOTCH3 expression in our integrated datasets may suggest an immunomodulatory mechanism of metastatic OS TAM-mediated suppression of anti-tumor T cell responses through paracrine Notch signaling which should be explored at the protein level in future studies.

Our data demonstrate that while intratumoral T cells exist in lower abundance compared to peritumoral regions, those that are present intratumorally exhibit a proliferative transcriptional profile. These findings suggest intratumoral T cells are receiving some degree of T cell activation signaling and perhaps reflects the presence of tumor-antigen specific T cells. To this end, we identify intratumoral T cells are enriched for CD44, a key surface protein which is upregulated with T cell activation [67]. Interestingly, this is observed alongside concurrent SPP1 expression in macrophages. The SPP1-CD44 axis is suggested to drive immune escape, T cell exhaustion, and subsequent immunotherapeutic resistance in a variety of carcinomas [68–70]. We also identify intratumoral enrichment for galectin-1 signaling, which plays a critical role in cellular adhesion to the ECM. Autocrine signaling through T cell secreted galectin-1 can promote induction of immune tolerance, exhaustion, apoptosis or skewing of T cell differentiation towards pro-tumorigenic Th2 and Treg phenotypes [71]. Overall, these findings identify cell-cell interactions and soluble mediators within the metastatic OS environment that may be driving suppression of effector T cell responses.

In parallel, we also identify metabolic mechanisms which may be reinforcing T cell dysfunction within the TME. CD73 is a known metabolic checkpoint expressed by Treg cells and

has been demonstrated to play an immunosuppressive role through its impacts on adenosine metabolism [72–74]. Our data further demonstrate intratumoral upregulation of *PKM* and *TPI1*, supporting an actively proliferating TME with reliance on glycolysis [75,76]. While intratumoral competition for glucose consumption has a known impact on T cell function, there is emerging evidence that the interplay between adenosine regulation and glycolysis also facilitates immune escape within the TME and can contribute to tumor progression [40,77]. We demonstrate this metabolically competitive landscape is conserved between species and may indicate a mechanism by which metastatic OS diminishes activated T cell efficacy. More work is warranted to validate if targeting adenosinergic or glycolytic signaling could enhance immunotherapeutic efficacy in metastatic OS.

MIF is a pleotropic immunoregulatory cytokine that has been previously demonstrated to be upregulated in OS and is associated with disease progression and poor patient outcomes [21,78,79]. Though normally produced by immune cells to enhance pro-inflammatory signals, elevated levels of MIF produced by tumor cells can inhibit T cell activation directly and indirectly through effects on macrophages and myeloid-derived suppressor cells [80–82]. Notably, in a syngeneic OS mouse model, concurrent MIF targeting potentiated the impact of PD-1 immunotherapy and increased pro-inflammatory tumor infiltrating macrophages and effector T cells [79]. MIF targeting also demonstrates direct anti-tumor effects, as evidenced by significantly reduced OS PDX tumor cell viability *in* vitro and reduced proliferation and metastasis of OS cells in xenograft mouse models [21,83]. Collectively, these studies and our findings support MIF as a compelling dual-compartment target for direct tumor targeting and disrupting the metastatic TME which drives therapeutic resistance.

Recent spatial profiling of pulmonary OS metastases in human cases shows unique activation of gene expression patterns contributing to the metastatic niche [21,22,84]. These studies have demonstrated increases in pro-fibrotic pathways associated with wound healing

505 and peripheralized immunologic activation which co-localized within increased density of pro-
506 inflammatory tissue-resident macrophages in the peri-tumoral stroma, bearing striking
507 similarities to those observed with a foreign body response. Here, we identify conservation of
508 these pro-inflammatory tissue-resident macrophages enriched within the peritumoral
509 microenvironment of canine OS lung metastases. These findings are particularly relevant, as
510 several myeloid-directed therapeutics which have demonstrated success in canine preclinical
511 trials have moved into the human setting [85–87]. Our data provide additional evidence of
512 conserved molecular features within the myeloid compartment of canine OS pulmonary
513 metastases, further supporting the utility of naturally occurring canine OS as a translationally
514 relevant model to study the OS metastatic TME.
515 All intratumoral compartments were enriched for *MMP14*, *PDGFRA*, *PRRX1*, and *TGFBI*
516 which are involved in a variety of ECM pathways and/or are key markers of cancer associated
517 fibroblasts [88–91]. Notably, MMP14 is an important collagenase for bone matrix formation and
518 osteogenic differentiation and its upregulation has been demonstrated in OS [92,93]. Both
519 PDGFRA and PRRX1 have been associated with pulmonary metastases in OS [94,95]. Lastly,
520 TGFBI derived from OS cells has also been associated with cellular migration and invasion,
521 providing cellular advantages in the metastatic environment [96]. Furthermore, TGFBI
522 expression in macrophages and stroma within the pulmonary environment has been associated
523 with reduced effector immune cell infiltration in cancer and inflammatory disease [97]. These
524 findings may emphasize necessary immune-matrix interactions important for infiltration and
525 mechano-responsiveness of immune cells within the TME [98,99]. Though many of these
526 pathways are not necessarily immune cell specific despite being expressed within our
527 intratumoral immune cell AOIs, these findings may highlight a challenge in deconvoluting spatial
528 data from matrix-dense tumors or cells with complex cytoplasmic morphology (e.g. macrophage,

fibroblast), whereby the GeoMx technology captures a 2D AOI from a 3D specimen, thus capturing matrix and/or cellular components from underlying z-planes.

Recent work has demonstrated that OS tumor and myeloid cells in the metastatic pulmonary environment perpetuate ECM remodeling for colonization [84]. Our work demonstrates these pro-fibrotic pathways are conserved between species and provides additional evidence that therapeutic targeting of fibrosis or CAFs may represent a viable strategy to treat metastasis and/or reverse immune suppression within the OS TME. We also demonstrate that effector immune cells which successfully infiltrate intratumorally may rely upon upregulation of matrix adhesion molecules. There is growing evidence mechanical factors of the ECM, such as stiffness, can profoundly impact immune cell function [99,100]. More research is warranted to better understand metastatic OS ECM composition and its influence on immune cell behavior.

There are a few important limitations to our study design which should be noted. First, there are currently no commercially available probe-based platforms for spatial whole transcriptome analysis in FFPE tissues of non-traditional species such as dogs. Compared to the human assay, the GeoMx probe-based panel for canine FFPE tissues is limited in coverage and heavily biased towards oncologic and immunologic targets in its design, which ultimately imparts skewing in differential gene and pathway analyses. Additionally, the cellular morphology markers used for AOI selection in this study were not perfectly matched across species, with the more pan-macrophage marker CD68 used in our human specimens and CD163 used in our canine tissues due to a lack of a species compatible CD68 antibody for canine FFPE samples. Although CD163 is also commonly used to identify macrophages in human tissue, the existing human specimens had already been profiled when the cross-species analysis was conceived. Despite this difference, both markers provided a means of identifying macrophage-enriched regions for subsequent analysis, and harmonization of antibodies could be a consideration for

future spatial profiling studies. Technical and probe-based limitations with the GeoMx platform were briefly discussed above and this likely contributed to limited cell type resolution from scRNASeq data. Another important limitation of this study is the use of Seurat for cross-species integration, which relies on a different statistical framework than the limma-based methods used in our independent analyses. Therefore, we cautiously interpreted integrated results and focused on contextualizing these findings alongside our independent analyses. Since sample AOI collections were not entirely balanced between canine and human cases, we recognize this may impart skewing of results towards certain individual specimens. This was briefly addressed in our interpretation of intratumoral T cell results and cell deconvolution findings. Future studies with more balanced sampling methods between canine and human groups would likely improve the robustness of these observations. Lastly, we show that spatial deconvolution using scRNAseq-derived annotations demonstrates distinct enrichment for select cell populations and complete absence of others. Interestingly, this enrichment was maintained in both species and irrespective of evaluable transcriptome size (i.e. whole transcriptome vs. canine ortholog-limited). This discrepancy may highlight distinct technologic differences in capturing cell-specific transcriptional resolution and challenges in integrating these technologies. Indeed, our findings suggest that both datasets require careful, complementary interpretation in relation to biologic relevance.

In conclusion, we successfully evaluated spatially dependent changes in tumor-associated T cell and macrophage infiltrates in canine lung metastatic OS samples using the GeoMx DSP platform. Moreover, we demonstrate a method of cross-species GeoMx spatial transcriptomic data integration which highlights regionally distinct immune cell heterogeneity that is conserved between canine and human metastatic OS, further strengthening the translational capabilities of the canine model. To this end, we specifically identify shared upregulation of a JAG1-Notch signaling pathway within intratumoral macrophages, metabolic alteration of intratumoral T cells, and intratumoral upregulation of MIF which warrant further

studies to evaluate their potential contribution towards metastatic OS progression and intratumoral immunosuppression.

REFERENCES

1. Fenger, J. M., London, C. A. & Kisseberth, W. C. Canine Osteosarcoma: A Naturally Occurring Disease to Inform Pediatric Oncology. *ILAR J.* **55**, 69–85 (2014).
2. Simpson, S., Dunning, M. D., de Brot, S., Grau-Roma, L., Mongan, N. P. & Rutland, C. S. Comparative review of human and canine osteosarcoma: morphology, epidemiology, prognosis, treatment and genetics. *Acta Vet. Scand.* **59**, 71 (2017).
3. Silver, K. I., Patkar, S., Mazcko, C., Berger, E. P., Beck, J. A. & LeBlanc, A. K. Patterns of metastatic progression and association with clinical outcomes in canine osteosarcoma: A necropsy study of 83 dogs. *Vet. Comp. Oncol.* **21**, 646–655 (2023).
4. Sheng, G., Gao, Y., Yang, Y. & Wu, H. Osteosarcoma and Metastasis. *Front. Oncol.* **11**, 780264 (2021).
5. Durfee, R. A., Mohammed, M. & Luu, H. H. Review of Osteosarcoma and Current Management. *Rheumatol. Ther.* **3**, 221 (2016).
6. J Burton, C. K. The role of clinical trials in veterinary oncology. *Vet. Clin. North Am. Small Anim. Pract.* **44**, 977–987 (2014).
7. LeBlanc, A. K. & Mazcko, C. N. Improving human cancer therapy through the evaluation of pet dogs. **20**, 727–742 (2020).
8. Oh, J. H. & Cho, J. Y. Comparative oncology: overcoming human cancer through companion animal studies. **55**, 725–734 (2023).
9. Simpson, S., Rizvanov, A. A., Jeyapalan, J. N., de Brot, S. & Rutland, C. S. Canine osteosarcoma in comparative oncology: Molecular mechanisms through to treatment discovery. *Front. Vet. Sci.* **9**, 965391 (2022).
10. Paoloni, M. & Khanna, C. Translation of new cancer treatments from pet dogs to humans. *Nat. Rev. Cancer* **8**, 147–156 (2008).
11. Decalf, J., Albert, M. L. & Ziai, J. New tools for pathology: a user's review of a highly multiplexed method for in situ analysis of protein and RNA expression in tissue. *J. Pathol.* **247**, 650–661 (2019).
12. Bassiouni, R., Gibbs, L. D., Craig, D. W., Carpten, J. D. & McEachron, T. A. Applicability of spatial transcriptional profiling to cancer research. *Mol. Cell* **81**, 1631–1639 (2021).
13. Parra, E. R. Methods to Determine and Analyze the Cellular Spatial Distribution Extracted From Multiplex Immunofluorescence Data to Understand the Tumor Microenvironment. *Front. Mol. Biosci.* **8**, 668340 (2021).
14. Beck, J. A., Garg, A., Church, S., Mazcko, C. & LeBlanc, A. K. Spatial Transcriptomics Advances the Use of Canine Patients in Cancer Research: Analysis of Osteosarcoma-

Bearing Pet Dogs Enrolled in a Clinical Trial. *Clinical Cancer Research* **31**, OF1–OF6 (2025).

15. Cronise, K. E., Coy, J., Dow, S., Hauck, M. L. & Regan, D. P. Immunohistochemical and transcriptomic characterization of T and myeloid cell infiltrates in canine malignant melanoma. *Vet. Comp. Oncol.* **22**, 377–387 (2024).

16. Danaher, P., Kim, Y., Nelson, B., Griswold, M., Yang, Z., Piazza, E. et al. Advances in mixed cell deconvolution enable quantification of cell types in spatial transcriptomic data. *Nature Communications 2022 13:1* **13**, 385- (2022).

17. Budhathoki, Y., Cannon, M. V., McEachron, T. A., Patel, A. G., Gust, M. J., Modiano, J. F. et al. Integrative Single-cell and Spatial Transcriptomic Analysis of Osteosarcoma Reveals Conserved and Distinct Ecosystems Across Sites and Species. *bioRxiv* 2026.01.13.698472 (2026) doi:10.64898/2026.01.13.698472.

18. Ortogero, N. & Yang, Z. Ortogero N, Yang Z (2021). GeomxTools: NanoString GeoMx Tools. R package version 2.0.0. *Bioconductor* (2021).

19. Song, Y., Miao, Z., Brazma, A. & Papatheodorou, I. Benchmarking strategies for cross-species integration of single-cell RNA sequencing data. *Nature Communications 2023 14:1* **14**, 1–17 (2023).

20. Zhong, H., Han, W., Gomez-Cabrero, D., Tegner, J., Gao, X., Cui, G. et al. Benchmarking cross-species single-cell RNA-seq data integration methods: towards a cell type tree of life. *Nucleic Acids Res.* **53**, (2025).

21. Eigenbrood, J., Wong, N., Mallory, P., Pereira, J. S., Williams, D., Morris, D. W. et al. Spatial Profiling Identifies Regionally Distinct Microenvironments and Targetable Immunosuppressive Mechanisms in Pediatric Osteosarcoma Pulmonary Metastases. *Cancer Res.* **85**, 2320–2337 (2025).

22. Ligon, J. A., Choi, W., Cojocaru, G., Fu, W., Hsiue, E. H. C., Oke, T. F. et al. Pathways of immune exclusion in metastatic osteosarcoma are associated with inferior patient outcomes. *J. Immunother. Cancer* **9**, e001772 (2021).

23. Sorenson, L., Fu, Y., Hood, T., Warren, S. & McEachron, T. A. Targeted transcriptional profiling of the tumor microenvironment reveals lymphocyte exclusion and vascular dysfunction in metastatic osteosarcoma. *Oncoimmunology* **8**, (2019).

24. Zuo, T., Xie, Q., Liu, J., Yang, J., Shi, J., Kong, D. et al. Macrophage-Derived Cathepsin S Remodels the Extracellular Matrix to Promote Liver Fibrogenesis. *Gastroenterology* **165**, 746-761.e16 (2023).

25. Kim, H. S. & Nam, J. S. The multifaceted role of YAP in the tumor microenvironment and its therapeutic implications in cancer. *Exp. Mol. Med.* **57**, 2201–2213 (2025).

26. Reggio, A., Fuoco, C., Deodati, R. & Palma, A. SPP1 macrophages across diseases: A call for reclassification? **39**, e70448 (2025).

27. Ding, W., Deng, S., Wang, Z., Chen, X., Xu, Z., Zhong, J. et al. CD163+ macrophages drive rapid pulmonary fibrosis via osteopontin secretion. *Int. Immunopharmacol.* **161**, 114976 (2025).

28. Sangaletti, S., Di Carlo, E., Gariboldi, S., Miotti, S., Cappetti, B., Parenza, M. et al. Macrophage-Derived SPARC Bridges Tumor Cell-Extracellular Matrix Interactions toward Metastasis. *Cancer Res.* **68**, 9050–9059 (2008).

29. Wong, S. L. I. & Sukkar, M. B. The SPARC protein: an overview of its role in lung cancer and pulmonary fibrosis and its potential role in chronic airways disease. *Br. J. Pharmacol.* **174**, 3 (2016).

30. Martínez, V. G., Rubio, C., Martínez-Fernández, M., Segovia, C., López-Calderón, F., Garín, M. I. et al. BMP4 Induces M2 Macrophage Polarization and Favors Tumor Progression in Bladder Cancer. **23**, 7388–7399 (2017).

31. Nguyen, A., Scott, M. A., Dry, S. M. & James, A. W. Roles of bone morphogenetic protein signaling in osteosarcoma. *International Orthopaedics 2014 38:11* **38**, 2313–2322 (2014).

32. Sergi, C. M. The role of SPARC/ON in human osteosarcoma. *Adv. Protein Chem. Struct. Biol.* **133**, 181–192 (2023).

33. Li, D., Masiero, M., Banham, A. H. & Harris, A. L. The Notch Ligand Jagged1 as a Target for Anti-Tumor Therapy. *Front. Oncol.* **4**, 254 (2014).

34. Zhang, Z., Wu, W. & Shao, Z. NOTCH Signaling in Osteosarcoma. *Curr. Issues Mol. Biol.* **45**, 2266 (2023).

35. Yu, F., Zhou, Q., Yu, W., Zhou, T., Cao, C., Xie, Y. et al. Tumor-associated macrophages promote chemoresistance to Paclitaxel via activating NOTCH2-JAG1 juxtacrine signaling. *Molecular Cancer 2026 25:1* **25**, 135- (2026).

36. Fujiwara, T., Yakoub, M. A., Chandler, A., Christ, A. B., Yang, G., Ouerfelli, O. et al. CSF1/CSF1R Signaling Inhibitor Pexidartinib (PLX3397) Reprograms Tumor-Associated Macrophages and Stimulates T-cell Infiltration in the Sarcoma Microenvironment. *Mol. Cancer Ther.* **20**, 1388–1399 (2021).

37. Ganjoo, S., Gupta, P., Corbali, H. I., Nanez, S., Riad, T. S., Duong, L. K. et al. The role of tumor metabolism in modulating T-Cell activity and in optimizing immunotherapy. *Front. Immunol.* **14**, 1172931 (2023).

38. Feng, Z., Ou, Y. & Hao, L. The roles of glycolysis in osteosarcoma. *Front. Pharmacol.* **13**, 950886 (2022).

39. Cao, X., Zhu, Z., Cao, Y., Hu, J. & Min, M. CD73 is a hypoxia-responsive gene and promotes the Warburg effect of human gastric cancer cells dependent on its enzyme activity. *J. Cancer* **12**, 6372 (2021).

40. Zhan, J., Huang, L., Niu, L., Lu, W., Sun, C., Liu, S. et al. Regulation of CD73 on NAD metabolism: Unravelling the interplay between tumour immunity and tumour metabolism. *Cell Commun. Signal.* **22**, 387 (2024).

41. Chen, S., Wainwright, D. A., Wu, J. D., Wan, Y., Matei, D. E., Zhang, Y. et al. CD73: an emerging checkpoint for cancer immunotherapy. *Immunotherapy* **11**, 983 (2019).

42. Deaglio, S., Dwyer, K. M., Gao, W., Friedman, D., Usheva, A., Erat, A. et al. Adenosine generation catalyzed by CD39 and CD73 expressed on regulatory T cells mediates immune suppression. *Journal of Experimental Medicine* **204**, 1257–1265 (2007).

43. Fang, F., Cao, W., Zhu, W., Lam, N., Li, L., Gaddam, S. et al. The cell-surface 5′-nucleotidase CD73 defines a functional T memory cell subset that declines with age. *Cell Rep.* **37**, 109981 (2021).

44. Xu, S., Yang, S., Sun, G., Huang, W. & Zhang, Y. Transforming Growth Factor-Beta Polymorphisms and Serum Level in the Development of Osteosarcoma. *DNA Cell Biol.* **33**, 802–806 (2014).

45. Chen, S., Fan, J., Zhang, M., Qin, L., Dominguez, D., Long, A. et al. CD73 expression on effector T cells sustained by TGF-β facilitates tumor resistance to anti-4-1BB/CD137 therapy. *Nature Communications 2019 10:1* **10**, 150- (2019).

46. Liu, Q., Song, M., Wang, Y., Zhang, P. & Zhang, H. CCL20-CCR6 signaling in tumor microenvironment: Functional roles, mechanisms, and immunotherapy targeting. *Biochimica et Biophysica Acta (BBA) - Reviews on Cancer* **1880**, 189341 (2025).

47. Yamazaki, T., Yang, X. O., Chung, Y., Fukunaga, A., Nurieva, R., Pappu, B. et al. CCR6 Regulates the Migration of Inflammatory and Regulatory T Cells. *J. Immunol.* **181**, 8391 (2008).

48. Yoshie, O. & Matsushima, K. CCR4 and its ligands: From bench to bedside. *Int. Immunol.* **27**, 11–20 (2015).

49. Marshall, L. A., Marubayashi, S., Jorapur, A., Jacobson, S., Zibinsky, M., Robles, O. et al. Tumors establish resistance to immunotherapy by regulating Treg recruitment via CCR4. *J. Immunother. Cancer* **8**, 764 (2020).

50. Lopez-Fuentes, E., Clugston, A. S., Lee, A. G., Sayles, L. C., Sorensen, N., Pons Ventura, M. V. et al. Epigenetic and transcriptional programs define osteosarcoma subtypes and establish targetable vulnerabilities. *Cancer Discov.* **16**, 296–319 (2025).

51. Liu, S., Zhang, Z., Wang, Z., Liu, C., Liang, G., Xu, T. et al. SPP1 Drives Colorectal Cancer Liver Metastasis and Immunotherapy Resistance by Stimulating CXCL12 Production in Cancer-Associated Fibroblasts. *Cancer Res.* **86**, 58–79 (2026).

52. Qi, J., Sun, H., Zhang, Y., Wang, Z., Xun, Z., Li, Z. et al. Single-cell and spatial analysis reveal interaction of FAP+ fibroblasts and SPP1+ macrophages in colorectal cancer. *Nature Communications 2022 13:1* **13**, 1742- (2022).

53. Zhang, Z., Liu, B., Lin, Z., Mei, L., Chen, R. & Li, Z. SPP1 could be an immunological and prognostic biomarker: From pan-cancer comprehensive analysis to osteosarcoma validation. *FASEB Journal* **38**, e23783 (2024).

54. Sun, B., Nishihira, J., Yoshiki, T., Kondo, M., Sato, Y., Sasaki, F. et al. Macrophage Migration Inhibitory Factor Promotes Tumor Invasion and Metastasis via the Rho-Dependent Pathway. *Clinical Cancer Research* **11**, 1050–1058 (2005).

55. Simpson, K. D., Templeton, D. J. & Cross, J. V. Macrophage Migration Inhibitory Factor Promotes Tumor Growth and Metastasis by Inducing Myeloid-Derived Suppressor Cells in the Tumor Microenvironment. *The Journal of Immunology* **189**, 5533–5540 (2012).

56. Schneider, K. L., Claus, L., Bucala, R. & Schulz-Heddergott, R. Targeting macrophage migration inhibitory factor as a potential therapeutic strategy in colorectal cancer. *Oncogenesis 2025 14:1* **14**, 30- (2025).

57. Corfe, S. A. & Paige, C. J. The many roles of IL-7 in B cell development; Mediator of survival, proliferation and differentiation. *Semin. Immunol.* **24**, 198–208 (2012).

58. Cool, T., Worthington, A., Poscablo, D., Hussaini, A. & Forsberg, E. C. Interleukin 7 receptor (IL7R) is required for myeloid cell homeostasis and reconstitution by hematopoietic stem cells. *Exp. Hematol.* **90**, 39 (2020).

59. Bikker, A., Erik Hack, C., P.J.G. Lafeber, F. & A.G. van Roon, J. Interleukin-7: a key Mediator in T Cell-driven Autoimmunity, Inflammation, and Tissue Destruction. *Curr. Pharm. Des.* **18**, 2347–2356 (2012).

60. Skerrett, S. J. Lysozyme in pulmonary host defense: new tricks for an old dog. *Am. J. Respir. Crit. Care Med.* **169**, 435–436 (2004).

61. Higgins, D. M., Basaraba, R. J., Hohnbaum, A. C., Lee, E. J., Grainger, D. W. & Gonzalez-Juarrero, M. Localized immunosuppressive environment in the foreign body response to implanted biomaterials. *American Journal of Pathology* **175**, 161–170 (2009).

62. Ivetic, A., Green, H. L. H. & Hart, S. J. L-selectin: A Major Regulator of Leukocyte Adhesion, Migration and Signaling. *Front. Immunol.* **10**, 1068 (2019).

63. Raffler, N. A., Rivera-Nieves, J. & Ley, K. L-selectin in inflammation, infection and immunity. *Drug Discov. Today Ther. Strateg.* **2**, 213–220 (2005).

64. Zhao, J., Zhang, X., Wang, G., Lin, Y., Liu, T., Chang, R. B. et al. Interpretable, flexible and spatially aware integration of multiple spatial transcriptomics datasets from diverse sources. *Nature Genetics 2026* 1–13 (2026) doi:10.1038/s41588-026-02579-x.

65. Guo, B., Ling, W., Kwon, S. H., Panwar, P., Ghazanfar, S., Martinowich, K. et al. Integrating Spatially-Resolved Transcriptomics Data Across Tissues and Individuals: Challenges and Opportunities. *Small Methods* **9**, 2401194 (2025).

66. Palaga, T., Wongchana, W. & Kueanjinda, P. Notch signaling in macrophages in the context of cancer immunity. *Front. Immunol.* **9**, 345656 (2018).

67. Baaten, B. J. G., Li, C. R. & Bradley, L. M. Multifaceted regulation of T cells by CD44. *Commun. Integr. Biol.* **3**, 508–512 (2010).

68. Klement, J. D., Paschall, A. V., Redd, P. S., Ibrahim, M. L., Lu, C., Yang, D. et al. An osteopontin/CD44 immune checkpoint controls CD8+ T cell activation and tumor immune evasion. *J. Clin. Invest.* **128**, 5549–5560 (2018).

69. Zhang, J., Peng, Q., Fan, J., Liu, F., Chen, H., Bi, X. et al. Single-cell and spatial transcriptomics reveal SPP1-CD44 signaling drives primary resistance to immune checkpoint inhibitors in RCC. *J. Transl. Med.* **22**, 1157 (2024).

70. Hou, L., Jiang, M., Li, Y., Cheng, J., Liu, F., Han, X. et al. Targeting SPP1+ macrophages via the SPP1-CD44 axis reveals a key mechanism of immune suppression and tumor progression in ovarian cancer. *Int. Immunopharmacol.* **160**, 114906 (2025).

71. Cedeno-Laurent, F. & Dimitroff, C. J. Galectin-1 research in T cell immunity: Past, present and future. *Clin. Immunol.* **142**, 107 (2011).

72. Yang, H., Yao, F., Davis, P. F., Tan, S. T. & Hall, S. R. R. CD73, Tumor Plasticity and Immune Evasion in Solid Cancers. *Cancers (Basel).* **13**, 177 (2021).

73. Da, M., Chen, L., Enk, A., Ring, S. & Mahnke, K. The Multifaceted Actions of CD73 During Development and Suppressive Actions of Regulatory T Cells. *Front. Immunol.* **13**, 914799 (2022).

74. Jarvis, L. B., Rainbow, D. B., Coppard, V., Howlett, S. K., Georgieva, Z., Davies, J. L. et al. Therapeutically expanded human regulatory T-cells are super-suppressive due to HIF1A induced expression of CD73. *Commun. Biol.* **4**, 1186 (2021).

75. Zahra, K., Dey, T., Ashish, Mishra, S. P. & Pandey, U. Pyruvate Kinase M2 and Cancer: The Role of PKM2 in Promoting Tumorigenesis. *Front. Oncol.* **10**, 159 (2020).

76. Jin, X., Wang, D., Lei, M., Guo, Y., Cui, Y., Chen, F. et al. TPI1 activates the PI3K/AKT/mTOR signaling pathway to induce breast cancer progression by stabilizing CDCA5. *J. Transl. Med.* **20**, 191 (2022).

77. Luengo, A., Li, Z., Gui, D. Y., Sullivan, L. B., Zagorulya, M., Do, B. T. et al. Increased demand for NAD+ relative to ATP drives aerobic glycolysis. *Mol. Cell* **81**, 691-707.e6 (2021).

78. Han, I., Lee, M. R., Nam, K. W., Oh, J. H., Moon, K. C. & Kim, H. S. Expression of Macrophage Migration Inhibitory Factor Relates to Survival in High-grade Osteosarcoma. *Clinical Orthopaedics and Related Research 2008 466:9* **466**, 2107–2113 (2008).

79. Chen, W., Liao, Y., Yao, H., Zou, Y., Fang, J., Zhang, J. et al. Multiomics integration analysis identifies tumor cell-derived MIF as a therapeutic target and potentiates anti-PD-1 therapy in osteosarcoma. *J. Immunother. Cancer* **13**, 11091 (2025).

80. Yan, X., Orentas, R. J. & Johnson, B. D. Tumor-derived macrophage migration inhibitory factor (MIF) inhibits T lymphocyte activation. *Cytokine* **33**, 188 (2006).

81. Wang, C., Zhou, X., Li, W., Li, M., Tu, T., Ba, X. et al. Macrophage migration inhibitory factor promotes osteosarcoma growth and lung metastasis through activating the RAS/MAPK pathway. *Cancer Lett.* **403**, 271–279 (2017).

82. Simpson, K. D. & Cross, J. V. MIF: metastasis/MDSC-inducing factor? *Oncoimmunology* **2**, (2013).

83. Zheng, L., Feng, Z., Tao, S., Gao, J., Lin, Y., Wei, X. et al. Destabilization of macrophage migration inhibitory factor by 4-IPP reduces NF-κB/P-TEFb complex-mediated c-Myb transcription to suppress osteosarcoma tumourigenesis. *Clin. Transl. Med.* **12**, e652 (2022).

84. Reinecke, J. B., Garcia, L. J., Gross, A. C., Cam, M., Cannon, M. V., Gust, M. J. et al. Aberrant Activation of Wound-Healing Programs within the Metastatic Niche Facilitates Lung Colonization by Osteosarcoma Cells. *Clinical Cancer Research* **31**, 414–429 (2025).

85. Kurzman, I. D., Shi, F., Vail, D. M. & MacEwen, E. G. In vitro and in vivo enhancement of canine pulmonary alveolar macrophages cytotoxic activity against canine osteosarcoma cells. *Cancer Biother. Radiopharm.* **14**, 121–128 (1999).

86. Meyers, P. A., Schwartz, C. L., Krailo, M. D., Healey, J. H., Bernstein, M. L., Betcher, D. et al. Osteosarcoma: The addition of muramyl tripeptide to chemotherapy improves overall survival - A report from the children's oncology group. *Journal of Clinical Oncology* **26**, 633–638 (2008).

87. Regan, D. P., Chow, L., Das, S., Haines, L., Palmer, E., Kurihara, J. N. et al. Losartan Blocks Osteosarcoma-Elicited Monocyte Recruitment, and Combined With the Kinase Inhibitor Toceranib, Exerts Significant Clinical Benefit in Canine Metastatic Osteosarcoma. *Clinical Cancer Research* **28**, 662–676 (2022).

88. Umar, M., Bartoletti, G., Dong, C., Gahankari, A., Browne, D., Deng, A. et al. Characterizing the role of Pdgfra in calvarial development. *Dev. Dyn.* **252**, 589 (2023).

89. Yu, H., Wergedal, J. E., Zhao, Y. & Mohan, S. Targeted disruption of TGFBI in mice reveals its role in regulating bone mass and bone size through periosteal bone formation. *Calcif. Tissue Int.* **91**, 81–87 (2012).

90. Lee, K. W., Yeo, S. Y., Gong, J. R., Koo, O. J., Sohn, I., Lee, W. Y. et al. PRRX1 is a master transcription factor of stromal fibroblasts for myofibroblastic lineage progression. *Nature Communications 2022 13:1* **13**, 2793- (2022).

91. Makutani, Y., Kawakami, H., Tsujikawa, T., Yoshimura, K., Chiba, Y., Ito, A. et al. Contribution of MMP14-expressing cancer-associated fibroblasts in the tumor immune microenvironment to progression of colorectal cancer. *Front. Oncol.* **12**, (2022).

92. Paiva, K. B. S. & Granjeiro, J. M. Matrix Metalloproteinases in Bone Resorption, Remodeling, and Repair. *Prog. Mol. Biol. Transl. Sci.* **148**, 203–303 (2017).

93. Ho, X. D., Phung, P., Q Le, V., H Nguyen, V., Reimann, E., Prans, E. et al. Whole transcriptome analysis identifies differentially regulated networks between osteosarcoma and normal bone samples. *Exp. Biol. Med.* **242**, 1802 (2017).

94. Xu, J., Xie, L. & Guo, W. PDGF/PDGFR effects in osteosarcoma and the “add-on” strategy. *Clin. Sarcoma Res.* **8**, 15 (2018).

95. Joko, R., Yamada, D., Nakamura, M., Yoshida, A., Takihira, S., Takao, T. et al. PRRX1 promotes malignant properties in human osteosarcoma. *Transl. Oncol.* **14**, 100960 (2020).

96. Yeh, L. T., Lin, C. W., Lu, K. H., Hsieh, Y. H., Yeh, C. Bin, Yang, S. F. et al. Niclosamide suppresses migration and invasion of human osteosarcoma cells by repressing TGFBI expression via the ERK signaling pathway. *Int. J. Mol. Sci.* **23**, (2022).

97. Lecker, L. S. M., Berlato, C., Maniati, E., Delaine-Smith, R., Pearce, O. M. T., Heath, O. et al. Tgfbi production by macrophages contributes to an immunosuppressive microenvironment in ovarian cancer. *Cancer Res.* **81**, 5706–5719 (2021).

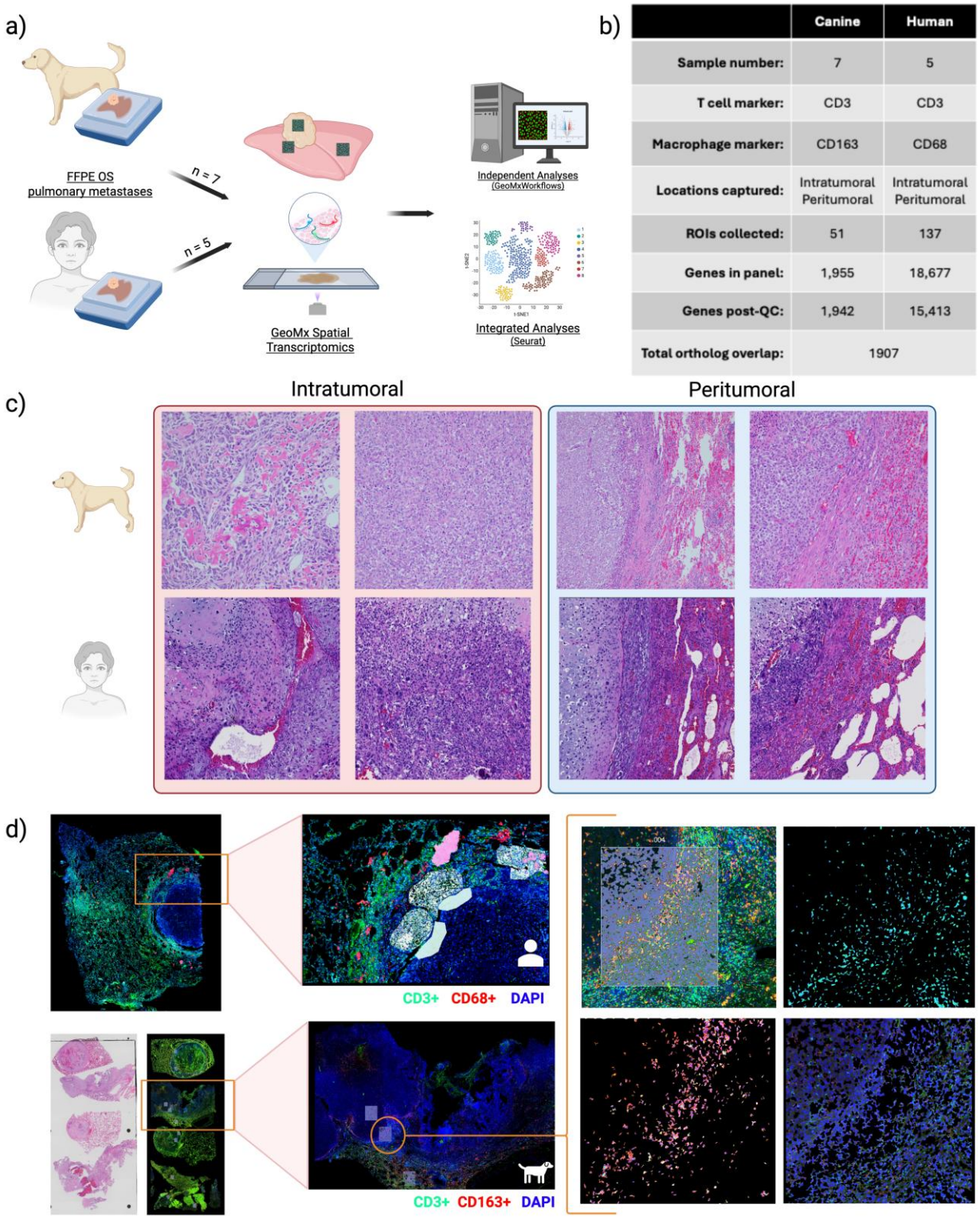
98. Cui, J., Dean, D., Hornicek, F. J., Chen, Z. & Duan, Z. The role of extracelluar matrix in osteosarcoma progression and metastasis. *Journal of Experimental & Clinical Cancer Research 2020 39:1* **39**, 1–11 (2020).

99. Du, W., Xia, X., Hu, F. & Yu, J. Extracellular matrix remodeling in the tumor immunity. *Front. Immunol.* **14**, 1340634 (2024).

100. Mai, Z., Lin, Y., Lin, P., Zhao, X. & Cui, L. Modulating extracellular matrix stiffness: a strategic approach to boost cancer immunotherapy. *Cell Death & Disease 2024 15:5* **15**, 1–16 (2024).

ETHICS DECLARATIONS

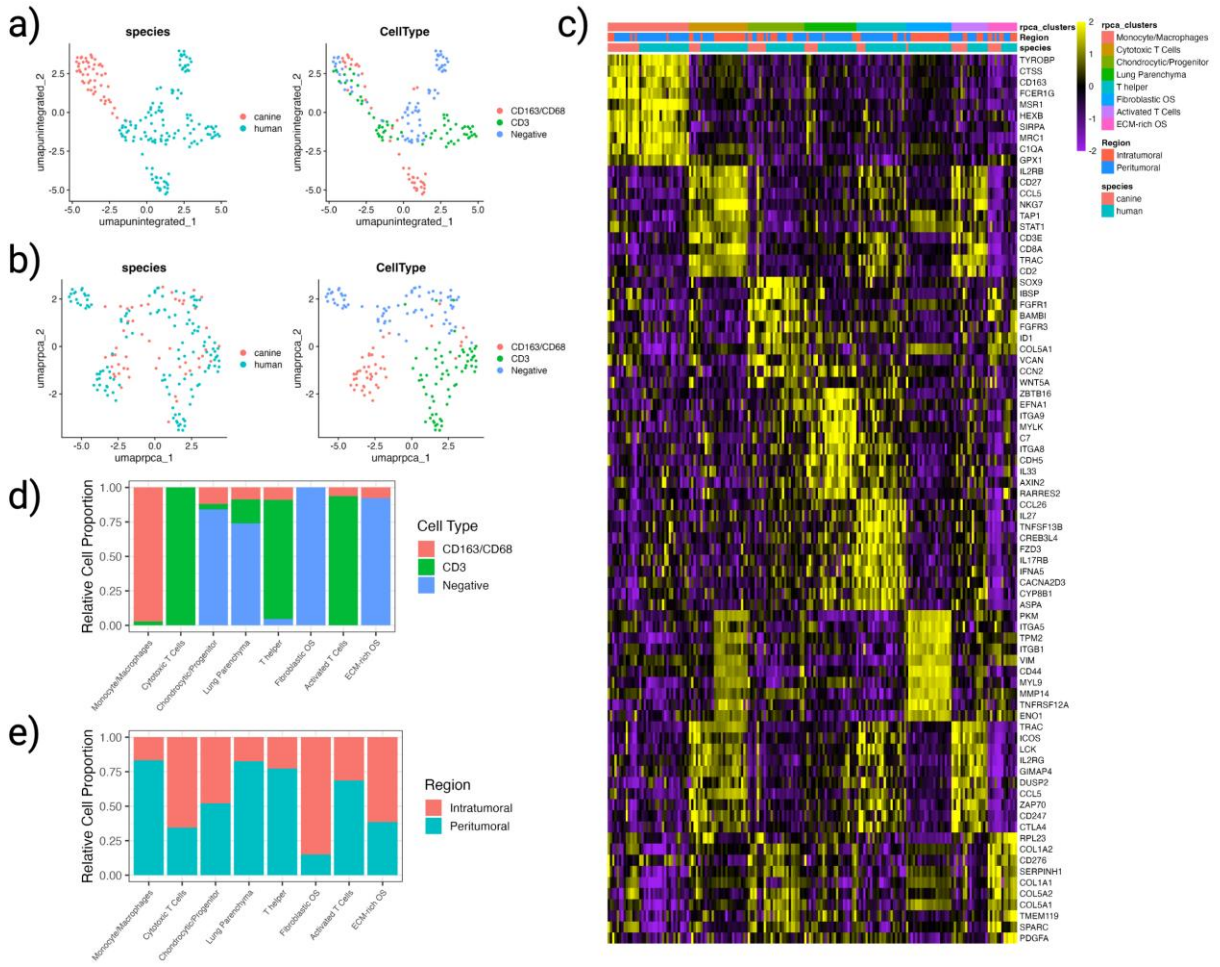
The authors declare no competing interests.



	Canine	Human
Sample number:	7	5
T cell marker:	CD3	CD3
Macrophage marker:	CD163	CD68
Locations captured:	Intratumoral Peritumoral	Intratumoral Peritumoral
ROIs collected:	51	137
Genes in panel:	1,955	18,677
Genes post-QC:	1,942	15,413
Total ortholog overlap:	1907	

Figure 1: Experimental Overview

a) Formalin-fixed, paraffin embedded (FFPE) canine (n = 7) or human (n = 5) pulmonary OS metastases were identified for GeoMx spatial transcriptomics and subsequent analysis using GeoMxWorkflows or integration with Seurat. b) Table with comparisons between canine and human panels and sample collection. c) Representative hematoxylin & eosin (H&E) sections of metastatic OS from canine and human samples utilized in this study. Intratumoral sections demonstrate diagnostic deposition of eosinophilic osteoid produced by pleomorphic spindle cells. Leading edge regions demonstrate compression of adjacent lung parenchyma and a variable peritumoral response including encapsulation and inflammation composed of lymphocytes, plasma cells, and macrophages. d) Geometric regions of interest (ROIs) were collected representing intratumoral and peritumoral locations. Segments collected (termed Areas of Illumination [AOI]) from each ROI included T cells (CD3+), macrophages (canine CD163+ or human CD68+), and remaining non-T-cell-non-macrophage ”Negative" tissues.



878

879 **Figure 2: Species integration of GeoMx data with Seurat preserves distinct cell**

880 **phenotypes and enhances T cell characterization**

881 a) UMAP dimensionality reduction of concatenated canine and human GeoMx datasets

882 demonstrates strong batch effect. Within each batch, there is sub clustering by AOI Cell

883 Type captured. b) UMAP dimensionality reduction of RPCA integrated GeoMx datasets

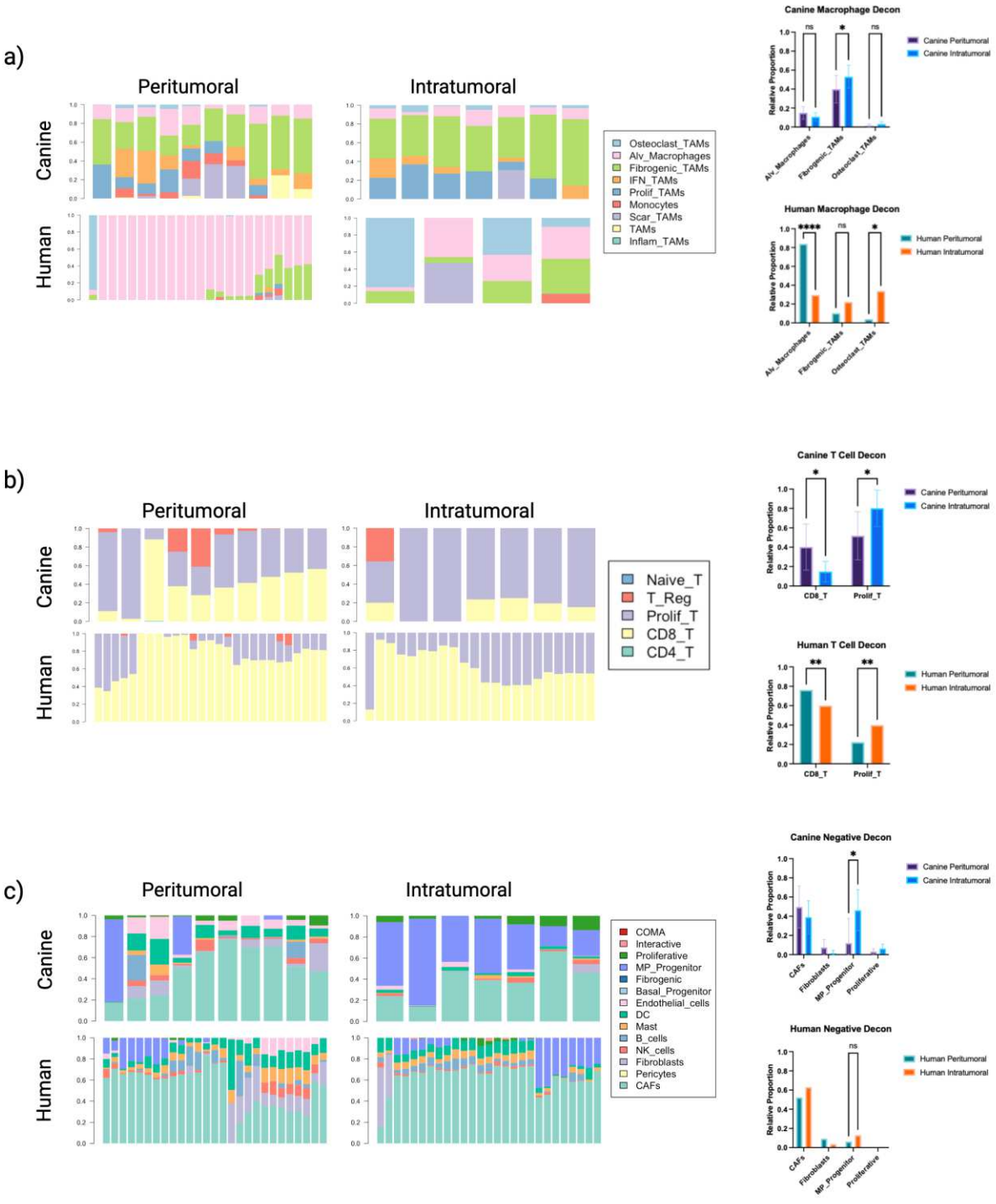
884 removes batch effects and demonstrates strong clustering by AOI Cell Type captured.

885 Interestingly, there is remnant species clustering within the CD163/CD68 cluster, likely

886 related to differences in the morphology markers utilized between species (CD68 for

887 human and CD163 for canine samples). c) Unsupervised RPCA clustering of the integrated

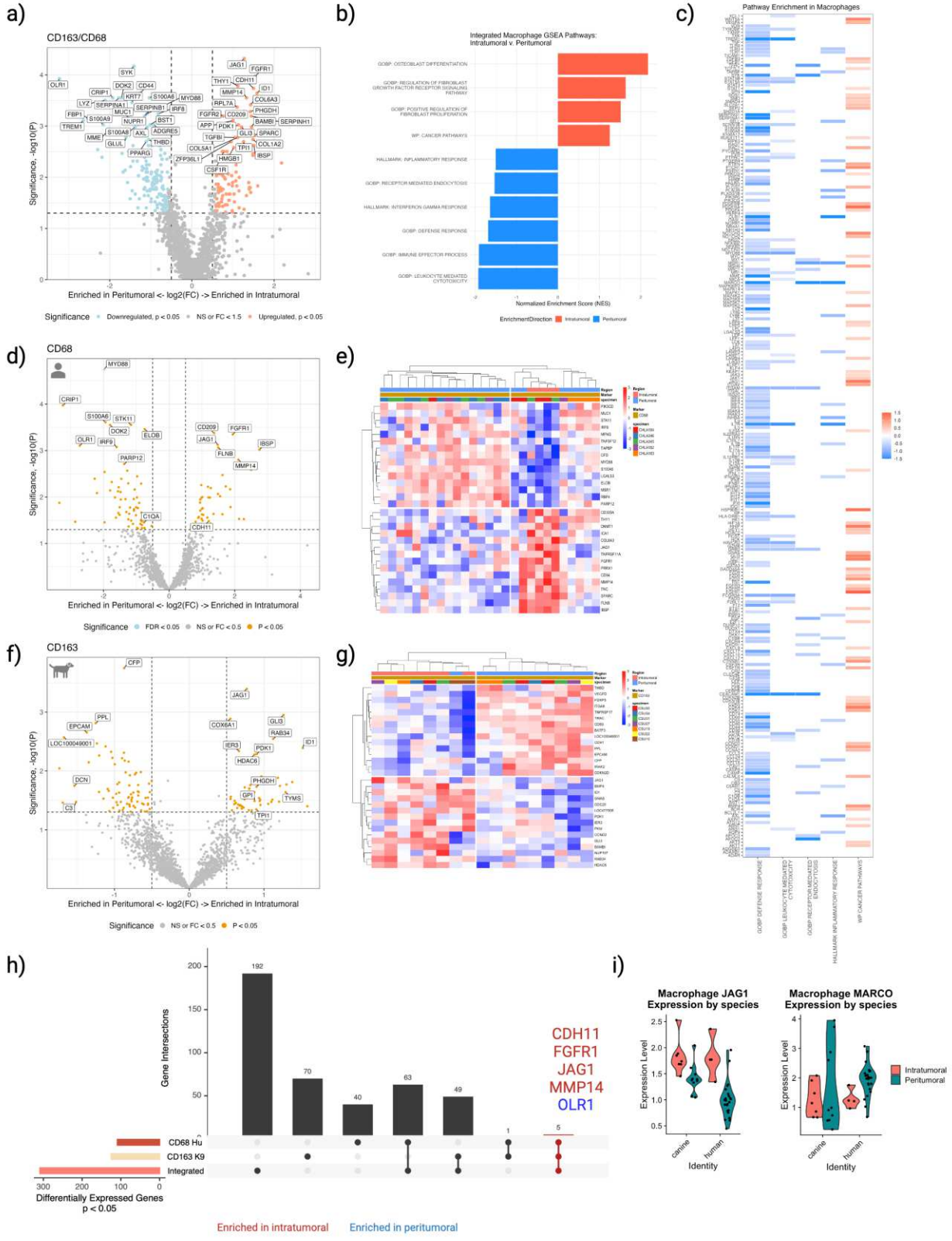
data demonstrated 8 distinct clusters which segregated strongly with cell identity. d) Relative proportion of Cell Type AOIs contributing to each unsupervised RPCA cluster identified e) Relative proportion of Region sampled contributing to each unsupervised RPCA cluster identified


a)
Peritumoral
Intratumoral
Canine
Human
Osteoclast_TAMs
Alv_Macrophages
Fibrogenic_TAMs
IFN_TAMs
Prolif_TAMs
Monocytes
Scar_TAMs
TAMs
Inflam_TAMs
Canine Macrophage Decon
Relative Proportion
Canine Peritumoral
Canine Intratumoral
Human Macrophage Decon
Human Peritumoral
Human Intratumoral
b)
Naive_T
T_Reg
Prolif_T
CD8_T
CD4_T
Canine T Cell Decon
Human T Cell Decon
c)
COMA
Interactive
Proliferative
MP_Progenitor
Fibrogenic
Basal_Progenitor
Endothelial_cells
DC
Mast
B_cells
NK_cells
Fibroblasts
Pericytes
CAFs
Canine Negative Decon
Human Negative Decon

893

Figure 3: Cell deconvolution demonstrates regionally distinct and highly heterogenous cell populations shared between canine and human metastatic OS

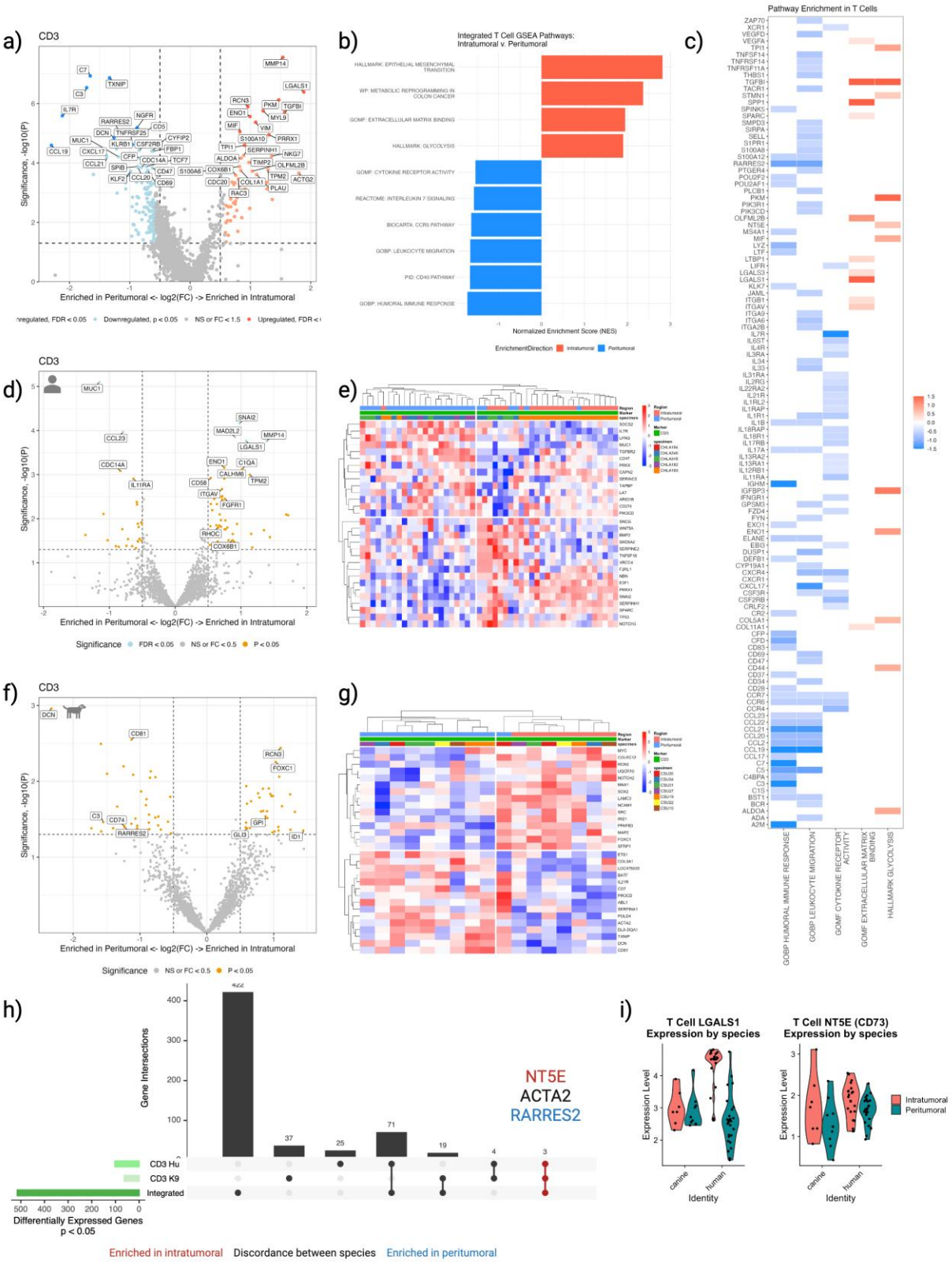
a) Deconvoluted macrophage peritumoral and intratumoral populations in canine and human OS metastases derived from scRNAseq whereby each bar represents a canine CD163+ AOI or human CD68+ AOI. Colors represent the relative proportions of cells derived from macrophage subcluster annotations from a multi-species OS scRNAseq atlas. Select relevant relative proportion changes are highlighted in adjacent bar graphs to emphasize regional differences and demonstrate statistical significance. b) Deconvoluted T cell peritumoral and intratumoral populations in canine and human OS metastases, whereby each bar represents a canine CD3+ AOI or human CD3+ AOI. Colors represent the relative proportions of cells derived from T cell subcluster annotations from a multi-species OS scRNAseq atlas. Select relevant relative proportion changes are highlighted in adjacent bar graphs to emphasize regional differences and demonstrate statistical significance. c) Deconvoluted “Negative” peritumoral and intratumoral populations in canine and human OS metastases, whereby each bar represents a canine CD163-CD3- AOI or human CD68-CD3- AOI. Colors represent the relative proportions of cell relevant annotations derived from a multi-species OS scRNAseq atlas. Select relevant relative proportion changes are highlighted in adjacent bar graphs to emphasize regional differences and demonstrate statistical significance.


a)
CD163/CD68
Significance, -log10(P)
Enriched in Peritumoral <- log2(FC) -> Enriched in Intratumoral
Significance Downregulated, p < 0.05 NS or FC < 1.5 Upregulated, p < 0.05
b)
Integrated Macrophage GSEA Pathways:
Intratumoral v. Peritumoral
GOBP: OSTEOBLAST DIFFERENTIATION
GOBP: REGULATION OF FIBROBLAST GROWTH FACTOR RECEPTOR SIGNALING PATHWAY
GOBP: POSITIVE REGULATION OF FIBROBLAST PROLIFERATION
WP: CANCER PATHWAYS
HALLMARK: INFLAMMATORY RESPONSE
GOBP: RECEPTOR MEDIATED ENDOCYTOSIS
HALLMARK: INTERFERON GAMMA RESPONSE
GOBP: DEFENSE RESPONSE
GOBP: IMMUNE EFFECTOR PROCESS
GOBP: LEUKOCYTE MEDIATED CYTOTOXICITY
Normalized Enrichment Score (NES)
EnrichmentDirection Intratumoral Peritumoral
c)
Pathway Enrichment in Macrophages
GOBP: DEFENSE RESPONSE
GOBP: LEUKOCYTE MEDIATED CYTOTOXICITY
GOBP: RECEPTOR MEDIATED ENDOCYTOSIS
HALLMARK: INFLAMMATORY RESPONSE
WP: CANCER PATHWAYS
d)
CD68
Significance, -log10(P)
Enriched in Peritumoral <- log2(FC) -> Enriched in Intratumoral
Significance FDR < 0.05 NS or FC < 0.5 P < 0.05
e)
f)
CD163
Significance, -log10(P)
Enriched in Peritumoral <- log2(FC) -> Enriched in Intratumoral
Significance NS or FC < 0.5 P < 0.05
g)
h)
Gene Intersections
192
70
40
63
49
1
5
CDH11
FGFR1
JAG1
MMP14
OLR1
CD68 Hu
CD163 K9
Integrated
Differentially Expressed Genes
p < 0.05
Enriched in intratumoral
Enriched in peritumoral
i)
Macrophage JAG1
Expression by species
Macrophage MARCO
Expression by species
Expression Level
canine
human
Identity
Intratumoral
Peritumoral

914

Figure 4: Independent and integrated analyses of macrophage AOIs in canine and human OS metastases demonstrates intratumoral macrophages are enriched for pro-tumorigenic JAG1 and trend towards more pro-fibrotic, immunosuppressive phenotypes

a) Volcano plot demonstrating 309 total DEGs in integrated dataset (n = 11 intratumoral and 33 peritumoral AOIs) b) Select significant GSEA pathways in integrated dataset c) Driving genes of select GSEA pathways in integrated dataset d) Volcano plot demonstrating 109 total DEGs in human dataset (n = 4 intratumoral and 23 peritumoral AOIs) e) Heatmap of the top and bottom 15 DEGs in the human dataset f) Volcano plot demonstrating 125 total DEGs in canine dataset (n = 7 intratumoral and 10 peritumoral AOIs) g) Heatmap of the top and bottom 15 DEGs in the canine dataset h) Upset plot demonstrating overlap between species integrating and independent DEG analyses. Genes which were identified as significant in both integrated and independent analyses are highlighted as text, with enrichment direction indicated by color. i) Violin plots demonstrating JAG1 expression separated by region and species


a)
CD3
Significance, -log10(P)
Enriched in Peritumoral <- log2(FC) -> Enriched in Intratumoral
Upregulated, FDR < 0.05
Downregulated, p < 0.05
NS or FC < 1.5
b)
Integrated T Cell GSEA Pathways:
Intratumoral v. Peritumoral
HALLMARK: EPITHELIAL MESENCHYMAL TRANSITION
WP: METABOLIC REPROGRAMMING IN COLON CANCER
GOMF: EXTRACELLULAR MATRIX BINDING
HALLMARK: GLYCOLYSIS
GOMF: CYTOKINE RECEPTOR ACTIVITY
REACTOME: INTERLEUKIN 7 SIGNALING
BIOCARTA: CCR5 PATHWAY
GOBP: LEUKOCYTE MIGRATION
PID: CD40 PATHWAY
GOBP: HUMORAL IMMUNE RESPONSE
Normalized Enrichment Score (NES)
EnrichmentDirection
Intratumoral
Peritumoral
c)
Pathway Enrichment in T Cells
GOBP HUMORAL IMMUNE RESPONSE
GOBP LEUKOCYTE MIGRATION
GOMF CYTOKINE RECEPTOR ACTIVITY
GOMF EXTRACELLULAR MATRIX BINDING
HALLMARK GLYCOLYSIS
d)
CD3
Significance, -log10(P)
Enriched in Peritumoral <- log2(FC) -> Enriched in Intratumoral
Significance
FDR < 0.05
NS or FC < 0.5
P < 0.05
e)
f)
CD3
Significance, -log10(P)
Enriched in Peritumoral <- log2(FC) -> Enriched in Intratumoral
Significance
NS or FC < 0.5
P < 0.05
g)
h)
Gene Intersections
NT5E
ACTA2
RARRES2
CD3 Hu
CD3 K9
Integrated
Differentially Expressed Genes
p < 0.05
Enriched in intratumoral
Discordance between species
Enriched in peritumoral
i)
T Cell LGALS1
Expression by species
T Cell NT5E (CD73)
Expression by species
Expression Level
canine
human
Identity
Intratumoral
Peritumoral

931

Figure 5: Independent and integrated analyses of T cell AOIs in canine and human OS metastases demonstrate conserved expression of immunosuppressive NT5E (CD73) and metabolic reprogramming pathways

a) Volcano plot demonstrating 515 total DEGs in integrated dataset (n = 29 intratumoral and 37 peritumoral AOIs) b) Biologically relevant, significant GSEA pathways in integrated dataset c) Driving genes of select GSEA pathways in integrated dataset d) Volcano plot demonstrating 103 total DEGs in human dataset (n = 22 intratumoral and 27 peritumoral AOIs) e) Heatmap of the top and bottom 15 DEGs in the human dataset f) Volcano plot demonstrating 59 total DEGs in canine dataset (n = 7 intratumoral and 10 peritumoral AOIs) g) Heatmap of the top and bottom 15 DEGs in the canine dataset h) Upset plot demonstrating overlap between species integrating and independent DEG analyses. Genes which were identified as significant in both integrated and independent analyses are highlighted as text, with enrichment direction indicated by color. i) Violin plots demonstrating LGALS1 and NT5E expression separated by region and species

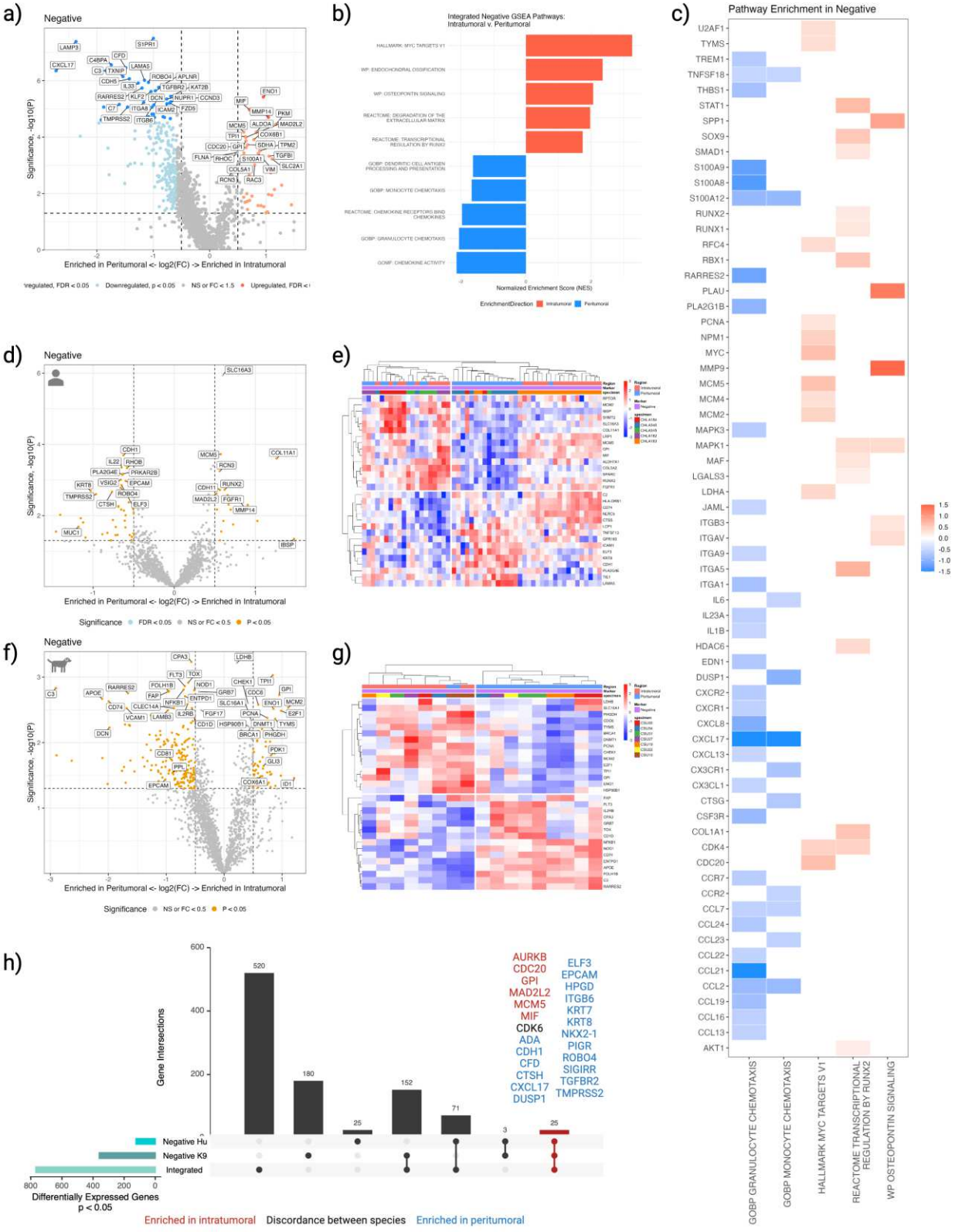

a)
Negative
Significance, -log10(P)
Enriched in Peritumoral <- log2(FC) -> Enriched in Intratumoral
b)
Integrated Negative GSEA Pathways:
Intratumoral v. Peritumoral
Normalized Enrichment Score (NES)
EnrichmentDirection Intratumoral Peritumoral
c)
Pathway Enrichment in Negative
GOBP GRANULOCYTE CHEMOTAXIS
GOBP MONOCYTE CHEMOTAXIS
HALLMARK MYC TARGETS V1
REACTOME TRANSCRIPTIONAL REGULATION BY RUNX2
WP OSTEOPONTIN SIGNALING
d)
Negative
Significance, -log10(P)
Enriched in Peritumoral <- log2(FC) -> Enriched in Intratumoral
Significance FDR < 0.05 NS or FC < 0.5 P < 0.05
e)
f)
Negative
Significance, -log10(P)
Enriched in Peritumoral <- log2(FC) -> Enriched in Intratumoral
Significance NS or FC < 0.5 P < 0.05
g)
h)
Gene Intersections
Negative Hu
Negative K9
Integrated
Differentially Expressed Genes
p < 0.05
AURKB CDC20 GPI MAD2L2 MCM5 MIF CDK6 ADA CDH1 CFD CTSH CXCL17 DUSP1
ELF3 EPCAM HPGD ITGB6 KRT7 KRT8 NKX2-1 PIGR ROBO4 SIGIRR TGFBR2 TMPRSS2
Enriched in intratumoral
Discordance between species
Enriched in peritumoral

Figure 6: Independent and integrated analyses of Negative AOIs in canine and human OS metastases demonstrate enrichment for pro-inflammatory and pro-tumorigenic MIF and the absence of leukocytic chemotactic signaling

a) Volcano plot demonstrating 768 total DEGs in integrated dataset (n = 34 intratumoral and 37 peritumoral AOIs) b) Select significant GSEA pathways in integrated dataset c) Driving genes of select GSEA pathways in integrated dataset d) Volcano plot demonstrating 124 total DEGs in human dataset (n = 27 intratumoral and 27 peritumoral AOIs) e) Heatmap of the top and bottom 15 DEGs in the human dataset f) Volcano plot demonstrating 360 total DEGs in canine dataset (n = 7 intratumoral and 10 peritumoral AOIs) g) Heatmap of the top and bottom 15 DEGs in the canine dataset h) Upset plot demonstrating overlap between species integrating and independent DEG analyses. Genes which were identified as significant in both integrated and independent analyses are highlighted as text, with enrichment direction indicated by color.

Supplementary Files

This is a list of supplementary files associated with this preprint. Click to download.

- S1.xlsx
- S2.xlsx
- S8.xlsx
- S3.xlsx
- SupplementalFigures.docx
- S5.xlsx
- S7.xlsx
- S6.xlsx
- S4.xlsx
- SupplementalFigures.pdf